Int. J. Electrochem. Sci., 14 **(2019)** 10259 – 10269, doi: 10.20964/2019.11.27

International Journal of
ELECTROCHEMICAL
SCIENCE
www.electrochemsci.org

Crystal Structure, Surface Activity and Corrosion Inhibition Effect of Dihydroxyethyl Ammonium O,O'-di(4-methylpheny) dithiophosphate for Q235 Steel in 1.0 M H_2SO_4

Chuan Lai[1,2,3*], *Jing Cao*[2], *Yuan-fang Deng*[2], *Ya-fei Yang*[2], *Xin Wen*[2], *Zhu-li Wang*[2], *Cheng-wu Fan*[1], *Ya-nan Shi*[1], *Ying Li*[1], *Jun-lan Li*[1], *Chang-lin Yang*[1], *Yi-jiu Yang*[1], *Wei Pang*[1], *Yang Liu*[1]

[1]School of Chemistry and Chemical Engineering, Sichuan University of Arts and Science, Dazhou 635000, China
[2]DaZhou Quality Technical Supervision and Inspection Testing Center, Dazhou 635000, China
[3]Laboratories of Fine Chemicals and Surfactants in Sichuan Provincial Universities, Sichuan University of Science and Engineering, Zigong, 643000, China
[*]E-mail: laichuanemail@163.com

Received: 16 June 2019 / *Accepted:* 10 August 2019 / *Published:* 7 October 2019

The hydrophilic corrosion inhibitor of dihydroxyethyl ammonium O,O'-di(4-methyl pheny)dithio-phosphate (DAOP) was synthesized. Meanwhile, the crystal structure, surface activity and corrosion inhibition of DAOP were presented in this work. The weight loss and potentiodynamic polarization measurements results all shows that DAOP is an effective hydrophilic corrosion inhibitor for Q235 steel (QS-235) in 1.0 M H_2SO_4. Potentiodynamic polarization measurements present that DAOP is a mixed-type inhibitor, which adsorbed on QS-235 surface attributable to both physisorption and chemisorption.

Keywords: Synthesis; Acid; Surface activity; Inhibitor; Chemisorption.

1. INTRODUCTION

Materials corrosion are presented in all fields of national economy. It is not difficult to find whether from daily life to transportation, chemical industry, machinery, metallurgy, or from cutting-edge science to national defense industry, all fields where materials are used, there corrosion problems are inevitable [1-5]. Corrosion will not only cause economic losses, but also cause the waste of resources and energy, as well as environmental pollution and potential safety risks [6-7].

Pickling corrosion as one of the classical corrosion, it can be slowed by using corrosion inhibitors, resulting from many advantages including economy, high efficiency and universality [8-10]. Many corrosion inhibitors with excellent corrosion inhibition properties are one-component organic

compounds, which can adsorb on the metal surface to form a protective film by the interaction between heteroatoms (S, N, P, O) and metal vacant orbitals [11-13]. It is necessary to develop new excellent organic corrosion inhibitor for protecting metal corrosion.

Based on the relationships between corrosion inhibition performance and inhibitors structures, the different compounds of O,O'-diaryldithiophosphates may be as effective inhibitors. In our previous studies, the O,O'- diaryldithiophosphates derivatives as excellent organic corrosion inhibitors were reported [14-16], however, all the reported compounds of O,O'-diaryldithiophosphates derivatives have the low solubility in aggressive medium (different acid solutions). In order to improve the solubility of O,O'-diaryldithiophosphates derivatives as corrosion inhibitors, some hydroxyl group (-OH) would be introduced into the molecular structure of corrosion inhibitor to improve its solubility, so dihydroxyethyl ammonium O,O'-di(4-methylpheny)dithio- phosphate (DAOP) would be prepared and characterized.

2. EXPERIMENTAL

2.1 Materials

Reagents, solvents and materials used in this work are described as follows: 4-methylphenol (4Me-PhOH), phosphorus pentasulphide (P_2S_5), toluene ($PhCH_3$), diethanolamine ($NH(CH_2CH_2OH)_2$) were used to synthesize the compound of dihydroxyethyl ammonium O,O'-di(4-methylpheny) dithiophosphate (DAOP, $[(4\text{-}MePhO)_2PS_2^-][H_2N^+(CH_2CH_2OH)_2]$) showing in figure 1. The concentrated sulfuric acid (H_2SO_4, 98%) was diluted as the corrosive solution (1.0 M H_2SO_4). The Q235 steel (QS-235, 0.785 cm^{-2}) electrode and test samples (20 mm × 50 mm × 6 mm, S = 28.4 cm^{-2}) used to evaluate corrosion inhibition performance. Moreover, the synthesized compound of DAOP was confirmed by Bruker SMART APEX CCD diffractometer.

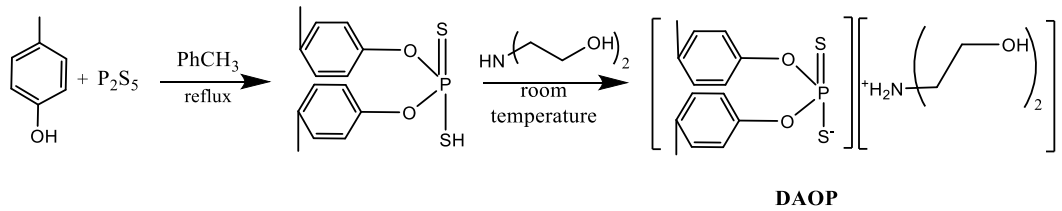

Figure 1. The synthesis of dihydroxyethyl ammonium O,O'-di(4-methylpheny) dithiophosphate (DAOP).

2.2 Performance evaluation

Surface activity evaluation: Surface tension was measured on A101Plus fully automatic surface tensiometer. Surface tension was used to evaluate the surface activity of DAOP as surfactants in double distilled water (surface tension 70.43 mN m^{-1}) at 30 °C.

Corrosion inhibition evaluation: (i) Potentiodynamic polarization measurement: the QS-235 electrode (working electrode), saturated calomel electrode (SCE, reference electrode) and platinum electrode (Pt electrode, counter electrode) as the triple-electrode system were choose to conduct

polarization measurement with the scan rate of 0.5 mV s^{-1}. The inhibition efficiency (IE_{PPM}, %) exhibited by polarization measurement was obtained using by equation (1) [17-18]. (ii) Weight loss measurement: This measurement was described in many studies [19-20]. Here, the inhibition efficiency (IE_{WLM}, %) and corrosion rate (v) were obtained from equation (2) and (3), where v is the corrosion rate, m is the mass of test samples, S is the superficial area of test samples (S = 28.4 cm^{-2}), t is time of immersion for corrosion.

$$IE_{\mathrm{PPM}}\ (\%) = \frac{i_0 - i_\mathrm{i}}{i_0} \times 100 \quad (1)$$

$$IE_{\mathrm{WLM}}\ (\%) = \frac{v_0 - v_i}{v_0} \times 100 \quad (2)$$

$$v_i = \frac{m_0 - m_\mathrm{i}}{St} \quad (3)$$

3. RESULTS AND DISCUSSION

3.1 Crystal structure of DAOP

A single crystal with dimensions 0.21 × 0.20 × 0.19 mm^3 for the hydrophilic compound of dihydroxyethyl ammonium O,O'-di(4-methylpheny) dithiophosphate (DAOP), was confirmed for structural determination at 150 K with the θ range of 2.535 - 25.010°.

Table 1. Crystallographic data of DAOP

Formula	$C_{18}H_{26}NO_4PS_2$
M	415.49
Crystal system	Monoclinic
Space group	$P2_1/c$
a /Å	11.680 (3)
b/Å	11.591 (3)
c/Å	16.390 (4)
β/°	107.345 (3)
V/$Å^3$	2118.0 (8)
Z	4
D_c/g cm^{-3}	1.303
μ /mm^{-1}	0.349
F(000)	880
GoF on F^2	1.016
R_1, wR_2 ($I>2\sigma(I)$) [a]	0.0371, 0.0933
R_1, wR_2 (all data) [a]	0.0519, 0.1018
$(\Delta\rho)_{max}$, $(\Delta\rho)_{min}$ /e $Å^{-3}$	0.321, -0.236
CCDC number	1908965

The numbers of observed and unique reflections are 14435 and 3723 (R_{int} = 0.0291). The data was integrated using the Siemens SAINT program [21]. The structure of DAOP was solved by direct method and refined on F^2 by full-matrix least-square using SHELXTL [22-25]. And crystallographic data, the selected bond and angles for DAOP were listed in table 1and 2.

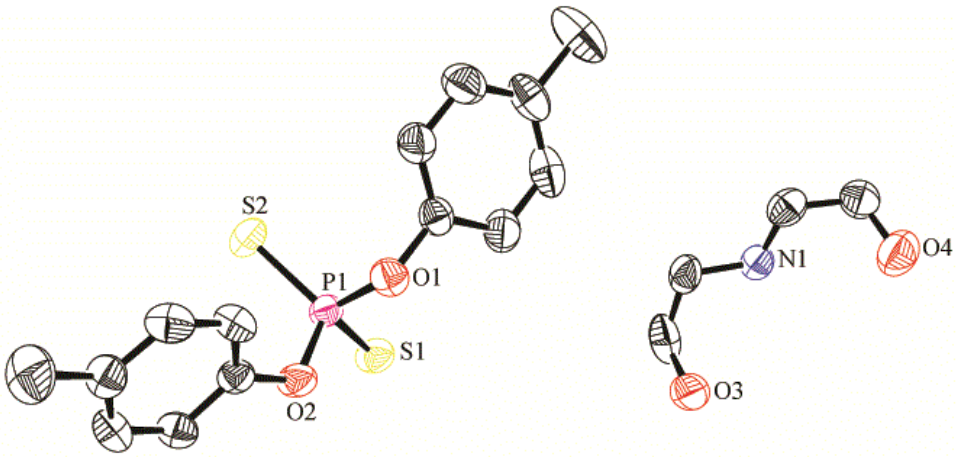

Figure 1. The crystal structure of DAOP.

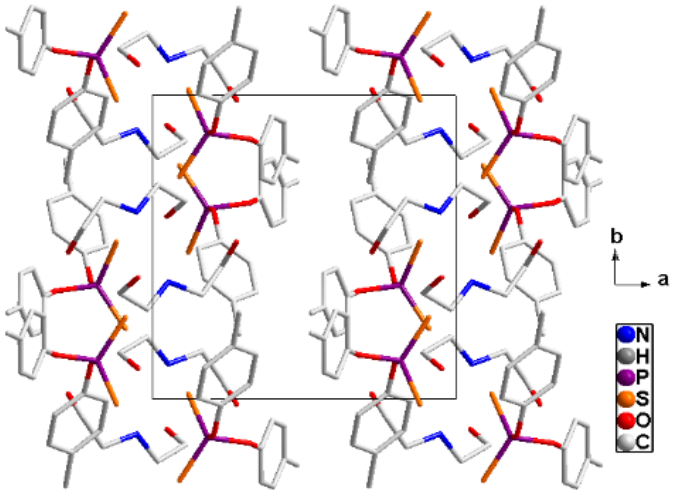

(a)

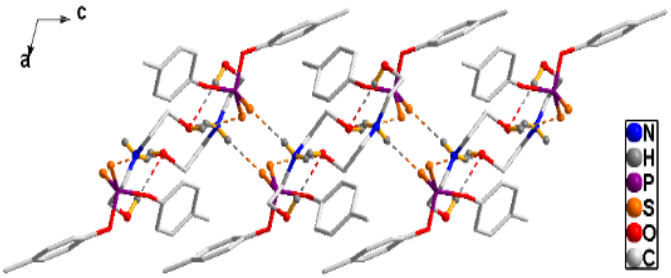

(b)

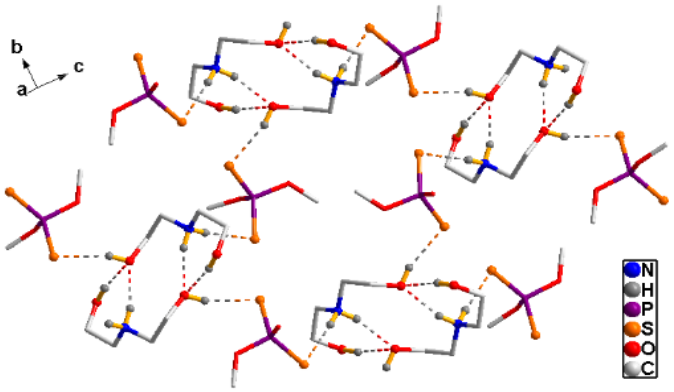

(c)

Figure 2. Packing diagram for DAOP viewed along the *c*-axis (a). The hydrogen bond networks for DAOP (b). The hydrogen bond networks within one layer of DAOP (c). All H atoms omitted for clarity in (a)-(c), the 4-MePh moieties also omitted in (c).

The crystal structure of DAOP was exhibited in figure 1. It can be found that DAOP crystallizes in monoclinic system with space group of $P2_1/c$. An expected distorted tetrahedral environment around phosphorus atom in the anion $[(4\text{-}MePhO)_2PS_2]^-$ can be clearly seen with two sulfur and two oxygen atoms making up the coordination sphere. Extensive weak hydrogen bond interactions were found among the anions $(4\text{-}MePhO)_2PS_2^-$ and cation $(HOCH_2CH_2)_2NH_2^+$ (figure 2 and table 3). The N1 … S2 and O3 … S1 hydrogen bonds, 3.378 (2) and 3.139 (2) Å, respectively, were formed for every molecular, and this N1 … S2 distance was consistent with those values of the analogous dithiophosphate ammonium salts $[Et_3NH]^+[(2\text{-}MeC_6H_4O)_2PS_2]^-$ (3.302 (2) Å) [26], $[Et_2NH_2]^+[(2\text{-}MeC_6H_4O)_2PS_2]^-$ (3.352(4) - 3.470(4) Å) [27], $[Et_3NH]^+[(2\text{-}MeC_6H_4O)_2PS_2]^-$ (3.286(6) and 3.211(6) Å) [28], $[Et_3NH]^+[(OCH_2CMe_2CH_2O)PS_2]^-$ (3.248(6) Å) [29]. Notably, every two cations $(HOCH_2CH_2)_2NH_2^+$ forms a dimer by O4 … O3 (3.307 (3) Å) and N1 … O3 (2.866 (3) Å) hydrogen bonds. These dimers were connected to anions $(4\text{-}MePhO)_2PS_2^-$ through O3 … S1, O4 ... S1, and N1 … S2 hydrogen bonds, forming a supramolecular layer in the *bc* plane (figure. 2b and 2c).

The bond lengths of P1 - S1 and P1 - S2 for DAOP were 1.9696 (9) and 1.9528 (8) Å, respectively, which was compared well with the analogous ammonium salts of O,O'-bis(aryl)dithiophosphates (1.942 (2) - 1.971 (2) [26-29] and cyclic dithiophosphates (1.945 (2) - 1.967 (2) Å) [33-34]. The S1 - P1 - S2 bond angle for DAOP was 116.70 (4)°, which was significantly smaller than those of $[Et_3NH]^+[(2\text{-}MePhO)_2PS_2]^-$(118.26 (3)°) [26], $[Et_2NH_2]^+[(4\text{-}MePhO)_2PS_2]^-$ (118.68 (7) and 118.61 (7)°) [27], $[Et_3NH]^+[(2\text{-}MePhO)_2PS_2]^-$ (118.62 (4)°) [28], $[Et_3NH]^+[(2,5\text{-}Me_2C_6H_3O)_2PS_2]$ (119.06 (5)°) [29], $[Et_3NH]^+[(OCH_2CMe_2CH_2O)PS_2]$ (119.8 (1) [30] or 119.27 (8) ° [31]), and $[Et_3NH]^+[CH_2\{6\text{-}t\text{-}Bu\text{-}4\text{-}MePhO\}_2PS_2]^-$ (121.03 (9)°) [31].

Table 2. The selected bond (Å) and angles (°) for DAOP.

O2 - P1	1.6110 (16)	O1 - C1	1.407 (3)
O1 - P1	1.6213 (17)	O2 - C8	1.402 (2)
S2 - P1	1.9528 (8)	O3 - C15	1.430 (4)
S1 - P1	1.9696 (9)	O4 - C18	1.395 (3)
O1 - P1 - O2	96.90 (9)	O1 - P1 - S1	110.33 (6)
S2 - P1 - O2	112.98 (6)	S2 - P1 - S1	116.70 (4)
S2 - P1 - O1	111.58 (7)	C1 -O1 - P1	121.29 (13)
S1- P1 - O2	106.49 (6)	C8 - O2 - P1	124.91 (13)

Table 3. The hydrogen bond parameters for DAOP.

D - H ... A	d(D - H) (Å)	d(H ... A) (Å)	d(D ... A) (Å)	<(D - H ... A) (°)
O(4) - H(4D) ... O(3) # 3	0.98	2.34	3.307 (3)	170.2
O(3) - H(3D) ... S(1) # 2	0.86	2.32	3.139 (2)	159.1
N(1) - H(1D) ... S(2) # 1	0.86	2.52	3.378 (2)	173.9
N(1) - H(1C) ... O(3) # 3	0.86	2.05	2.866 (3)	158.2
O(4) - H(4D) ... S(1) # 4	0.98	2.85	3.368 (2)	113.7
N(1) - H(1C) ... O(3)	0.86	2.57	2.978 (3)	110.3

3.2 Surface activity

The effect of concentrations on surface tension for DAOP in double distilled water at 30 °C was presented in figure 3. It was not difficult to find that as the concentration of DAOP increases, the surface tension decreases and finally tends to be stable. Meanwhile, the observation was recorded for DAOP up to critical micelle concentration, which can be used to calculate critical micelle concentration of DAOP. The data of critical micelle concentration was obtained from the break point in the surface tension - log *C* plots, which was 40.04 mmol L^{-1}. Moreover, the γ_{cmc} (surface tension) at critical micelle concentration was 32.18 mN m^{-1}. The π_{cmc} (maximum surface pressure) can be calculated by the following equation: $\pi_{cmc} = \gamma_0 - \gamma_{cmc}$, where γ_0 is 70.43 mN m^{-1}, and the π_{cmc} is 38.25 mN m^{-1}. Based on the above results, which shown that DAOP is an excellent surfactant.

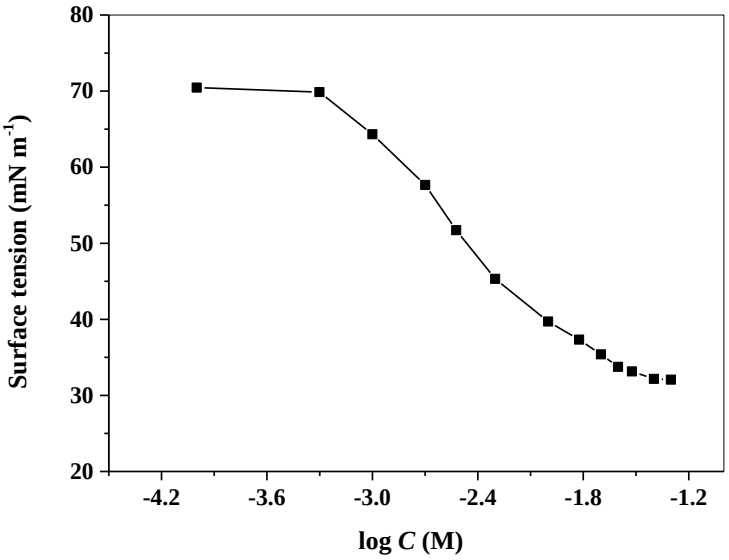

Figure 3. The effect of concentrations on surface tension for DAOP in double distilled water at 30 °C.

3.3 Potentiodynamic polarization measurement

The potentiodynamic polarization curves and their polarization parameters for QS-235 corrosion in 1.0 M H_2SO_4 in the absence and presence of different concentration (0 - 100 mg L^{-1}) of DAOP at 30 °C were revealed in figure 4 and table 4. From this figure and table, it can be found that the cathodic curves and anodic curves all shift to lower current densities for QS-235 corrosion in1.0 M H_2SO_4 with different concentration (0 - 100 mg L^{-1}) of DAOP. At the same time, it can be clearly seen from table 4, that there is a significant difference in corrosion current density between 1.0 M H_2SO_4 with and without DAOP.

Table 4. The polarization parameters for QS-235 in 1.0 M H_2SO_4 in the absence and presence of different concentration (0 - 100 mg L^{-1}) of DAOP at 30 °C.

c(mg L^{-1})	E(mV)	ΔE(mV)	i (μA cm^{-2})	β_a(mV dec^{-1})	β_c(mV dec^{-1})	IE_{PPM}(%)
0	-475	-	2936.0	137	150	-
20	-455	20	846.0	134	139	71.2
40	-447	28	370.5	129	134	87.4
60	-433	42	146.6	125	122	95.0
80	-430	45	35.94	118	118	98.8
100	-420	55	10.57	114	117	99.6

Here, the current density is much higher for QS-235 in 1.0 M H_2SO_4 absence of DAOP comparing with which presence of DAOP, and current density increases with DAOP concentration decreasing. In addition, it can be found both cathodic and anodic Tafel slopes (β_c and β_a) decreased with DAOP increasing. With DAOP concentration increased to 80 mg L^{-1} and 100 mg L^{-1}, the IE_{PPM} (%) reach to 98.8% and 99.6%, respectively. The high inhibition efficiency indicates that DAOP is a

new excellent corrosion inhibitor for QS-235 in 1.0 M H_2SO_4. In addition, according to the changes of corrosion potential to distinguish the types of corrosion inhibitors, it found that all the corrosion potential changes (ΔE) were less than 60 mV, which indicated that DAOP as the corrosion inhibitor is a mixed-type inhibitor [6, 14,15,16].

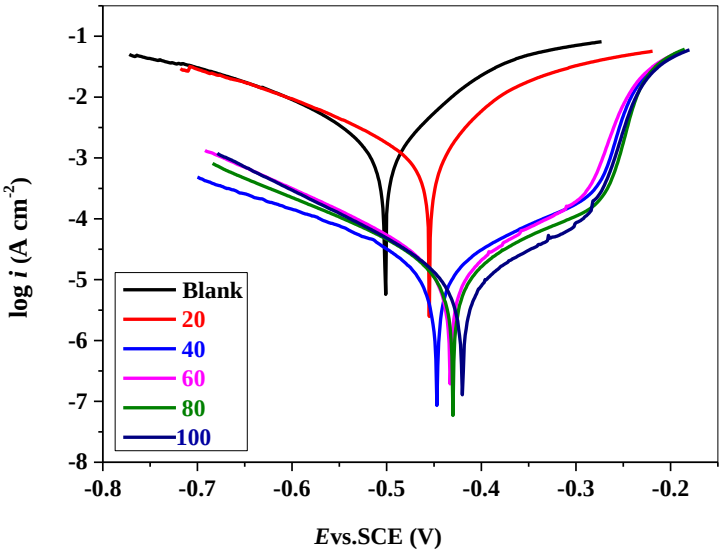

Figure 4. The potentiodynamic polarization curves for QS-235 in 1.0 M H_2SO_4 in the absence and presence of different concentration (0 - 100 mg L^{-1}) of DAOP at 30 °C.

3.4 Weight loss measurement and adsorption isotherms

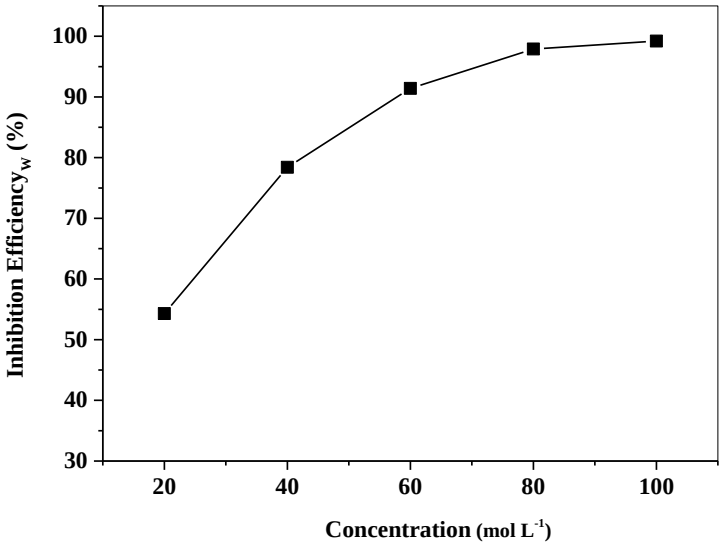

Figure 5. The inhibition efficiency (IE_W, %) for QS-235 in 1.0 M H_2SO_4 with different concentration (0 - 100 mg L^{-1}) of DAOP 30 °C.

The inhibition efficiency (IE_W, %) for QS-235 in 1.0 M H_2SO_4 with different concentration (0 - 100 mg L^{-1}) of DAOP 30 °C was presented in figure 5. It was obvious that, the IE_W (%) increased with the concentration of DAOP increasing, when the concentration of DAOP increase to 80 mg L^{-1}, the IE_W (%) change slightly with the concentration continuously increases. With the concentration of DAOP increased to 100 mg L^{-1}, that the IE_W (%) was 99.2%, which also demonstrate that DAOP is an excellent corrosion inhibitor for QS-235 in H_2SO_4 solution.

Meanwhile, the data showing in figure 5 were used for fitting to describe the adsorption behavior of DAOP on QS-235 surface in 1.0 M H_2SO_4 [37-38]. Although different adsorption isotherms can be selected to describe the adsorption behavior of corrosion inhibitors, only Langmuir adsorption isotherm is most suitable for describing the adsorption of DAOP on QS-235 surface in 1.0 M H_2SO_4 seeing in equation (4), (5) and figure 6. From figure 6, it can be found that has a good linear relationship between c/θ and c, and the value of R^2 obtained by fitting is 0.99482. The value of R^2 close to 1 indicated that the adsorption of DAOP on QS-235 surface in 1.0 M H_2SO_4 is suitable to be described by Langmuir adsorption isotherm. In addition, the adsorption free energy (ΔG_a^0) can be calculated by equation (6), (7) and fitting results (seeing in figure 6), which was -35.23 (kJ mol^{-1}). The ΔG_a^0 is higher than -40.00 kJ mol^{-1} (-35.23 kJ mol^{-1}) indicated that the adsorption of DAOP on QS-235 surface belongs to physisorption and chemisorption [6, 39-40].

$$\frac{c}{\theta} = \frac{1}{K} + c \quad (4)$$

$$\theta = \frac{v_0 - v_i}{v_0} \quad (5)$$

$$\Delta G_a^0 = -RT\ln(55.5K_a) \quad (6)$$

$$K_a = M_{DAOP} \times K \times 10^3 = \frac{415\times10^3}{19.58} = 2.1195 \times 10^4 \text{ (mol L}^{-1}\text{)} \quad (7)$$

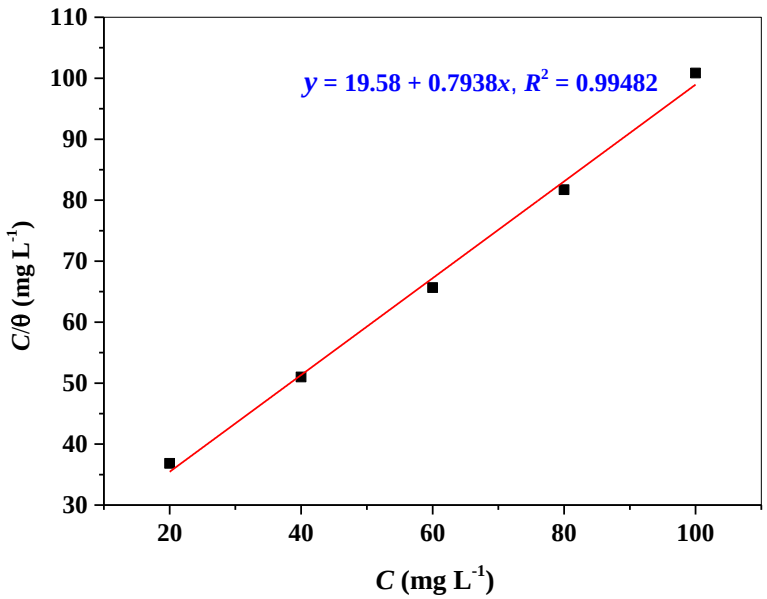

Figure 6. Langmuir adsorption plots for QS-235 in 1.0 M H_2SO_4 with different concentration (0 - 100 mg L^{-1}) of DAOP 30 °C.

4. CONCLUSIONS

1. A novel hydrophilic corrosion inhibitor of dihydroxyethyl ammonium O,O'-di(4-methyl-pheny)dithiophosphate (DAOP) was successfully synthesized and characterized by single crystal X-ray diffraction.

2. DAOP is an excellent surfactant, which C_{cmc} is 40.041 mmol L^{-1}.

3. The results obtained from weight loss methods were in good agreement with that measured from potentiodynamic polarization measurements, which shown that DAOP is an effective hydrophilic corrosion inhibitor.

4. DAOP is a mixed-type corrosion inhibitor. The adsorption of DAOP on QS-235 surface obeys Langmuir isotherm, which is a mixed adsorption.

ACKNOWLEDGMENTS

This project is supported by Dazhou Scientific Research Project (18ZDYF0009), Laboratories of Fine Chemicals and Surfactants in Sichuan Provincial Universities (2016JXZ03, 2018JXZ01), Sichuan University of Arts and Science (2018KC005Z, 2018SCL001Z).

References

1. J. V. Nardeli, C.S. Fugivara, M. Taryba, E. R. P. Pinto and A.V. Benedetti, *Prog. Org. Coat*.,135 (2019) 368.
2. T. Zhang, W. Jiang, H. Wang and S. Zhang, *Mater. Chem. Phys*., 13 (2019) 121866.
3. V. N. Ayukayeva, G. I. Boiko, N. P. Lyubchenko, R. G. Sarmurzina and S. A. Dergunov, *Colloid. Surface.A: Physicochem. Eng. Aspects,* 579 (2019) 123636.
4. C. M. Fernandes, T. S. F. Fagundes, N. E. Santos, T. S. M. Rocha and E .A. Ponzio, *Electrochimica Acta,* 312 (2019) 137.
5. M. Balonis, G. Sant and O. B. Isgor, *Cement Concre. Comp*., 101 (2019) 15.
6. C. Lai, B. Xie and X. Guo, *Phosphorus, Sulfur*, 2019 (2019)1.
7. Q. Wang, B. Tan, H. Bao, Y. Xie, Y. Mou, P. Li, D. Chen, Y. Shi, X. Liand W. Yang, *Bioelectrochemistry,* 128 (2019) 49.
8. I. B. Obot, I. B. Onyeachu, N. Wazzan and A. H. Al-Amri, *J. Mol. Liq*., 279 (2019) 190 .
9. M. Wang, J. Zhang, Q. Wang and M.Du, Int. *J. Electrochem. Sci.*, 14 (2019) 8852.
10. C. J. Zhang, X. Lu, J. Zhang, L. Zhang, C. Zhu, Y. Zhang and T. Wu, *Int. J. Electrochem. Sci.*, 14 (2019) 8601.
11. Y. Lu, W. Wang, C. Zhang and J. Zhao, *Int. J. Electrochem. Sci.*, 14 (2019) 8579.
12. I. B. Obot, S. A. Umoren and N. K. Ankah, *J. Mol. Liq*., 277 (2019) 749.
13. W. Zhang, Z. Zhang, W. Li, X. Huang, L. Ruan and L. Wu, *Int. J. Electrochem. Sci.,* 14 (2019) 7348.
14. C. Lai, X. Guo, J. Wei, B. Xie, L. Zou, X. Li, Z. Chen, C. Wang, *Open Chem*., 15 (2017) 263
15. C. Wang, C. Lai, B. Xie, X. G. Guo, D. Fu, B. Li and S. Zhu, *Results Phys*., 10 (2018) 558.
16. C. Lai, B. Xie, L. Zou, X. Zheng, X. Ma, S. Zhu, *Results Phys*., 7 (2017) 3434.
17. W. Gou, W. Wang, W. Xie, P. Zhang, L. Wang, J. Zhang, Y. Shi and B. Xie, *Int. J. Electrochem. Sci.*, 14 (2019) 7947.
18. M. Mobin, M. Basik and J. Aslam, *Measurement* 134 (2019) 595.
19. Z. Sanaei, M. Ramezanzadeh, G. Bahlakeh and B. Ramezanzadeh, *J. Ind. Eng. Chem*. 69 (2019) 18.
20. M. Javidi, R. Chamanfar and S. Bekhrad, *J. Nat. Gas Scie. Eng*. 61 (2019) 197.

21. Bruker AXS Inc. APEX-II (ver. 2008.1-0), SAINT (ver. 7.51A) and SADABS (ver. 2007/4); Bruker AXS Inc.: Madison, WI, USA, 2008.
22. SHELXTL (version 5.0), Reference manual, Siemens Industrial Automation, Analytical Instruments, Madison, WI, 1995.
23. G. M. Sheldrick. *Acta Crystallogr.*, A64 (2008) 112.
24. G. M. Sheldrick. *Acta Crystallogr.*, C71 (2015) 3.
25. Sheldrick G. M. SHELXL 2017/1. University of Göttingen: Göttingen, Germany, 2017.
26. A. L. Bingham, J. E. Drake, C. Gurnani, M. B. Hursthouse, M. E. Light, M. Nirwan and R. Ratnani, *J. Chem. Crystallogr.*, 36 (2006) 627.
27. B. Xie, C. Lai, Y. G. Xiang, K. Zou, Z. Xiang, C. Huang and B.Yi, *Chin. J. Applied Chem.*, 29 (2012) 200.
28. J. E. Drake, C. L. B. Macdonald, A. Kumar, S. K. Pandey and R. Ratnani. *J. Chem. Crystallogr.*, 35 (2005) 447.
29. M. Kour, S. Kumar, A. Feddag, S. Andotra, A. Chouaih, V. K. Gupta., R. Kant and S. K. Pandey, *J. Mol. Struct.*, 1157 (2018) 708.
30. A. Kumar, J. Dinesh, S. Kour, M. S. Hundal and S. K. Pandey *J. Chem. Crystallogr.*, 42 (2012): 299.
31. K. C. Swamy, S. Kumarasyamy, S. Raja, *J. Chem. Crystallogr.*, 3 1(2001) 51.
32. I. S. Pohrebova and T. M. Pylypenko, *Mater. Today: Proc*. 6 (2019) 192.
33. M. Murmu, S. K. Saha, N. C. Murmu and P. Banerjee, *Corros. Sci.* 146 (2019) 134.
34. L. T. Popoola, *Heliyon*, 5 (2019) e01143.
35. G. Vasyliev, V. Vorobiova, *Mater. Today: Proc.,* 6 (2019) 178.